Available online at www.sciencedirect.com

SCIENCE DIRECT®

ELSEVIER

Nuclear Instruments and Methods in Physics Research A ▮ (▮▮▮▮) ▮▮▮–▮▮▮

NUCLEAR INSTRUMENTS & METHODS IN PHYSICS RESEARCH Section A

www.elsevier.com/locate/nima

# Investigation of a solid-state photodetector

D. Beznosko, G. Blazey, D. Chakraborty, A. Dyshkant, K. Francis, D. Kubik, J.G. Lima, V. Rykalin*, V. Zutshi

*Northern Illinois University, DeKalb, IL 60115, USA*

Received 28 September 2004; received in revised form 27 January 2005; accepted 5 February 2005

**Abstract**

We present results on the operation and performance characteristics of the MRS (metal/resistor/semiconductor) photodiode. These include measurements of threshold characteristics, noise frequency, dependence of signal amplitude on the applied voltage and temperature, and stability as a function of time and radiation dose. The single photoelectron separation for this photosensor is demonstrated with a light emitting diode. The response of the photodetector to light produced in a scintillator is studied with cosmic ray muons and a $^{106}$Ru source. In addition, fiber-sensor alignment issues were evaluated. The results are promising and illustrate the potential use of MRS as photosensors in high-energy physics detectors.



*PACS:* 29.40.Wk; 29.40.Mc; 29.40.Vj

*Keywords:* Solid-state photosensor; Geiger mode; Multi-pixel; Characteristics; Irradiation; Miniaturized photodetector



## 1. Introduction

Calorimeters, optimized for particle flow algorithms, are under active study for their promise of delivering superior jet energy resolution, essential to exploiting the full physics potential of a future $e^+e^-$ linear collider. These calorimeters require fine longitudinal and transverse segmentation to efficiently resolve the showers initiated by the individual particles constituting a jet. For designs with small scintillating cells as the active medium [1], the large channel count imposes strong constraints on the cost and performance of photodetectors. This has directed our attention to solid-state photomultipliers working in the avalanche mode [2]. In spite of their relatively short history, these photodetectors may have an impact on the design of future detectors. For instance, photodetectors that are embedded in the scintillator reduce light loss and routing problems by eliminating the need for long clear fibers to carry the light from the scintillating material to the

*Corresponding author. Tel.: +1 815 753 3504.
*E-mail address:* rykalin@fnal.gov (V. Rykalin).

0168-9002/$ - see front matter 
doi:10.1016/j.nima.2005.02.023

photodetector. This is possible since these MRS solid-state photodetectors are small in size and are expected to perform well in strong magnetic fields.

The MRS photodiode is a multi-pixel solid-state device with every pixel operating in the limited Geiger multiplication mode. Avalanche quenching is achieved by a resistive layer on the sensor surface. The device has about 1500 pixels per $1\times1\,\mathrm{mm}^2$ sensor [2]. The detection efficiency of the device reaches 25% at 500 nm [3]. In this paper we have concentrated on the operating parameters and stability of the MRS; i.e., the dependence of amplification and noise count rate on the applied bias voltage, temperature and radiation dose. These parameters are important in a system with millions of channels. Also, the linearity of response was measured.

## 2. Experimental section

### 2.1. Working point

MRS amplification, detection efficiency and intrinsic noise directly depend on the applied bias voltage, and this dependence varies from one individual photodetector to another. Thus, a particular bias voltage (working point) must be chosen for the above parameters.

The apparatus used to study these parameters is shown schematically in Fig. 1a. An eight-channel MRS board with preamplifiers from the Center for Perspective Technologies and Apparatus (CPTA) [2] serves as the MRS output amplifier and signal shaper (Fig. 1b). Each channel includes an MRS sensor, a bias voltage tuner and a preamplifier. Initially, all channels were tested under identical conditions with the same bias voltage and the same light signal from a green light emitting diode (LED) with peak emission at ~510 nm. The MRS was excited by a LED; the signal was amplified, discriminated and recorded. The light from the same LED had been applied to each individual channel by physically switching the position of the fiber; thus similar responses were expected. Results from a few representative channels are shown in Fig. 2. The disparity of response observed indicates that the optimal bias voltage must be found and tuned individually for each channel. Also Fig. 2 demonstrates that the MRS is sensitive to single photoelectrons.

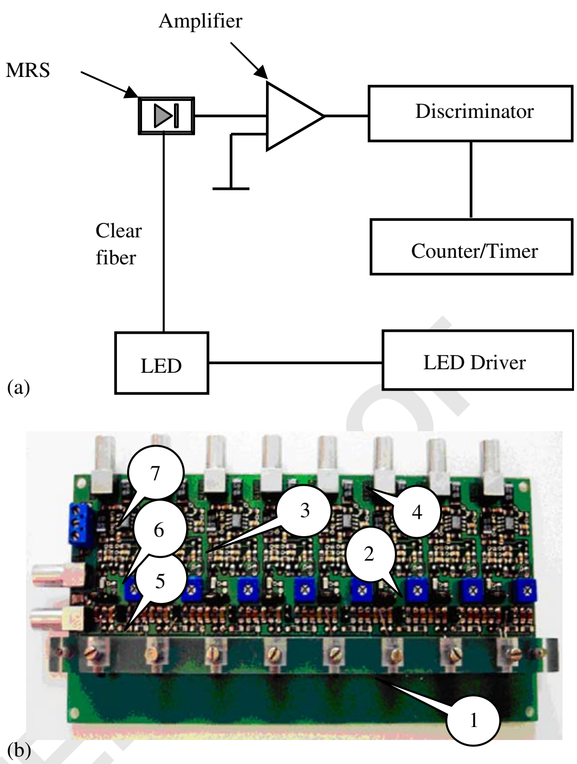


Fig. 1. (a) Block diagram showing the apparatus used for choosing the working point. (b) Eight-channel MRS board: 1—MRS sensor, 2—bias voltage tuner, 3—preamplifier, 4—signal output, 5—bias voltage input, 6—test signal input and 7—preamplifier power.

For further studies, channel #4 was selected. A LeCroy [4] 623B octal discriminator and an ORTEC [5] 872 quad counter/timer were used to process the signal. Unless stated otherwise, all measurements were carried out at $22.6\pm0.2\,^{\circ}\mathrm{C}$. The following tests were used to determine a working point for the sensor.

#### 2.1.1. Noise count rate and bias voltage

First, a low frequency (~150 Hz) signal was applied to the LED that illuminated the photodetector through a clear fiber, and the noise rate was measured as a function of the applied bias voltage. The bias voltage was measured at the

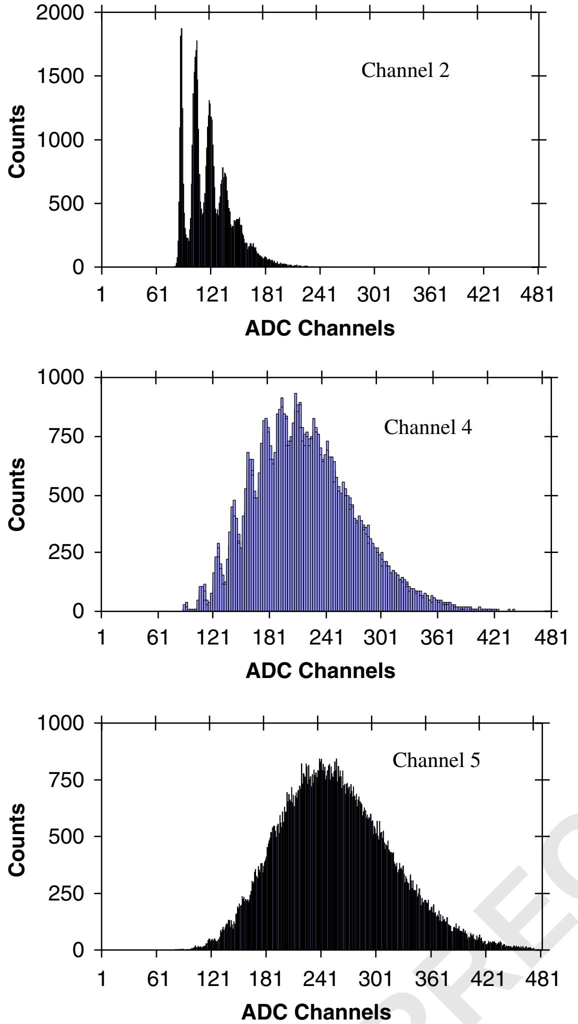


Fig. 2. Response of channels 2, 4 and 5 to the same LED signal for identical bias voltages. Because of the spread in optimal bias voltage values for each MRS, high levels of noise mask the PE structure for some channels.

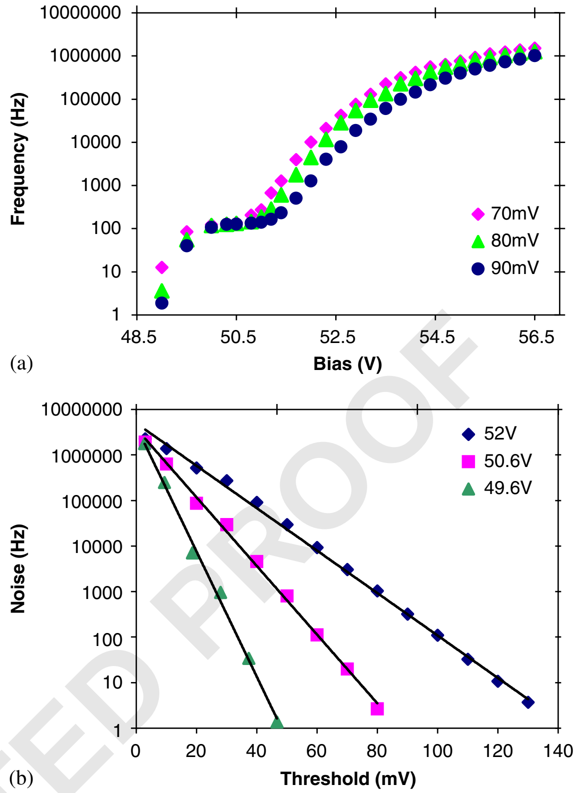


Fig. 3. (a) Count rate dependence on bias voltage for thresholds of 70, 80 and 90 mV (~150 Hz signal from LED is supplied to MRS). (b) Dark rate dependence on the threshold for different bias voltages. At 49.6 V we have 1 PE ~24 mV, at 50.6 V—1 PE ~30 mV, at 52 V—1 PE ~38 mV. The LED was off for this measurement.

MRS directly. The preamplifier output was connected to a discriminator that, in turn, was connected to a counter/timer (Fig. 1). Counts were accumulated over a period of 1 min and converted into frequency. Fig. 3a shows the output signal frequency versus the bias voltage for three different threshold values (70, 80 and 90 mV). These values were chosen so that the amplitude of the sensor's response is larger than the value of the thresholds for the majority of the bias voltages.

Fig. 3b shows the MRS dark noise rate as a function of the threshold applied for a set of bias voltages. These measurements were done for three different bias voltages. For illustrative purposes, the bias voltages chosen are at the beginning of the plateau (49.6 V), at its end (50.6 V) and at some point outside but not too far from the plateau (52.0 V). We can see that while the MRS dark rate can be high (in MHz range), for a given voltage setting, it is a steeply falling function of the threshold applied. For thresholds in the 70–90 mV and bias voltages in the 49.6–50.6 V range, there is minimal contribution from the dark noise. Thus, the plateau (from ~50.0 to ~51.0 V) in Fig. 3a is a region of full signal detection with the least number of counts from noise (the observed count rate is close to the pulse rate of the LED) for a chosen threshold range.

At higher bias voltages, keeping the threshold value fixed, the noise becomes prominent and starts to dominate the count rate. We start seeing noise signals with two and even three photoelectrons (PE) (here 1 PE corresponds to 24–38 mV, depending on the bias voltage). Thus for higher bias voltage values the plateau will be obtained for higher threshold values. In the MRS, 1 PE corresponds to the firing of one pixel. A pixel can fire if a photon is detected and an avalanche is initiated. In addition, if a thermal electron–hole pair is created in the photosensitive area of the cell, this cell will also fire exactly as in the case of photon detection, producing the "single photoelectron" noise. Note that at higher bias voltages the curve in Fig. 3a starts to level again. This effect is due to the resistive layer at the top of the sensor that limits the gain and noise increase correspondingly. Gain limiting behavior will be illustrated in the next subsection.

### 2.1.2. Amplification and bias voltage

In the second set of studies, an ~150 Hz constant amplitude signal was applied to a green LED (maximum emission at ~510 nm), illuminating the photodetector through a clear fiber. Then the bias voltage was varied, and the amplitude of the output signal was measured and plotted as a function of the bias voltage (Fig. 4a).

After some value of the bias voltage, a further increase in the voltage does not yield an increase in amplification. This indicates that gain is limited. This bias value can be used as a definition of the working point. However, at such high bias voltages the detector is close to the breakdown voltage; it generates high-frequency noise that might not be suitable for some applications (see Fig. 3a).

In addition, measurements of the average noise level as a function of the biasing voltage were conducted. The LED was disconnected from the pulse generator, but the generator was still producing the gates to start the ADC. The

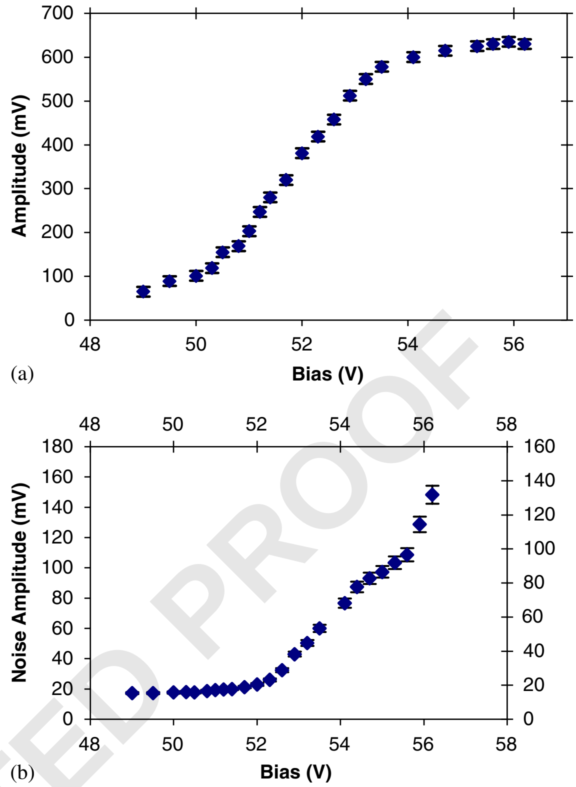


Fig. 4. (a) Signal amplitude as a function of the bias voltage for MRS excited with an LED. (b) Average noise amplitude as a function of the bias voltage for an unilluminated MRS.

pedestal—subtracted mean noise amplitudes were plotted in Fig. 4b.

### 2.1.3. Signal-to-noise ratio and bias voltage

To illustrate the balance between amplification and noise, the signal-to-noise (S/N) ratio was calculated at each value of bias voltage, taking the ratio of the data in Fig. 4a and b. The results are plotted in Fig. 5; a distinct maximum may be taken as the optimal balance between the level of sensor noise and amplification. The bias voltage value for the MRS, obtained in this test, was used for cosmic ray and radioactive source measurements. From Fig. 5 the optimal bias voltage for the MRS sensor used is 52.0 V. In addition, the working points have been measured for 10 more sensors

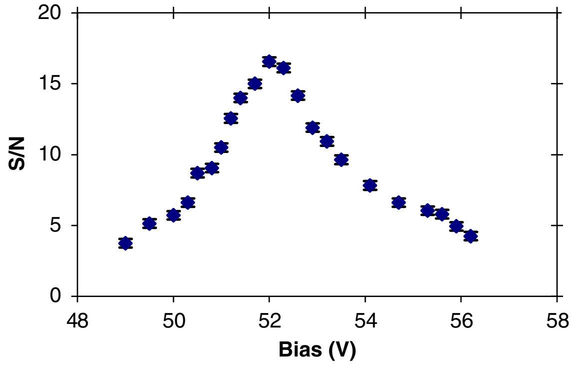


Fig. 5. Signal-to-noise ratio as a function of the bias voltage.

from the same production batch. The average was 51.89 ± 0.35 V.

### 2.2. *MRS time stability at the working point*

To determine the stability of the working point for the MRS, a LED signal was supplied to the sensor and a noise count rate taken at the set voltage. After 20 h, the noise count rate was taken again and compared to the initial one (LED signal was at 58 Hz, temperature from the beginning to the end of the test was 22.8 ± 0.1 °C). Initially, at 50.40 ± 0.01 V with the discriminator set at 80 mV threshold, the MRS count rate was 68.7 ± 1.1 Hz (averaged over a 3 min period). After 20 h of continuous operation, a 69.2 ± 1.1 Hz noise rate was measured (also averaged over 3 min). The rates measured are compatible within the estimated uncertainties.

### 2.3. *Temperature effects*

The dependence of noise and signal on temperature was measured. For the temperature tests, the setup shown in Fig. 1 was used in the same manner as for the measurements of the noise characteristics and the amplification dependence on bias voltage. The threshold (80 mV) and the bias voltage (51.3 V) were kept fixed while the temperature varied. The exponential behavior of the noise frequency expected is illustrated in Fig. 6a. The fit is added to emphasize the exponential

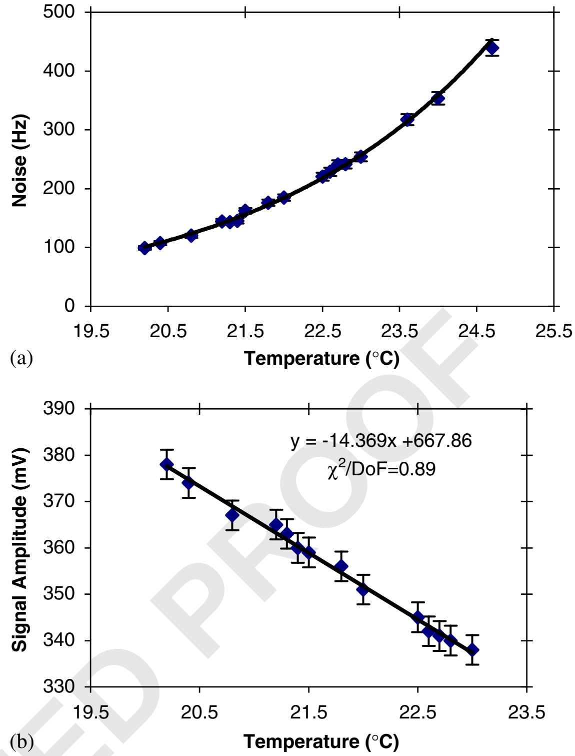


Fig. 6. (a) Noise frequency vs. temperature; (b) signal amplitude vs. temperature.

relationship between the noise frequency and the temperature.

The amplitude dependence on temperature was also studied. The results of this test are presented in Fig. 6b. The behavior of the signal amplitude is linear for the range of temperatures for which data were obtained. Shown in Fig. 6b are the best fit and its empirical formula. The observed signal loss is ~3.5% per degree increase in temperature.

### 2.4. *Irradiation effects*

A separate study was undertaken to observe changes, if any, in the MRS sensor response after irradiation with a 1 Mrad dose of gamma rays. The sensor noise, amplification, signal detection, and bias voltage range were measured before and after irradiation. The "before" measurements are all presented in the previous sections. Noise measurements are illustrated in Fig. 3b. Signal detection is presented in Fig. 3a. Finally, amplification and bias voltage range for the sensor are shown in Fig. 4. Any major changes to these characteristics would indicate damage to the internal cell structure of the sensor. Fig. 7a, b and c show the point-by-point ratios of each plot in Figs. 3a, b, and 4 to the equivalent ones measured after the MRS sensor was irradiated. Within experimental uncertainties, all the ratios are very close to 1, indicating that a 1 Mrad dose of gamma radiation causes no detectable damage to the sensor.

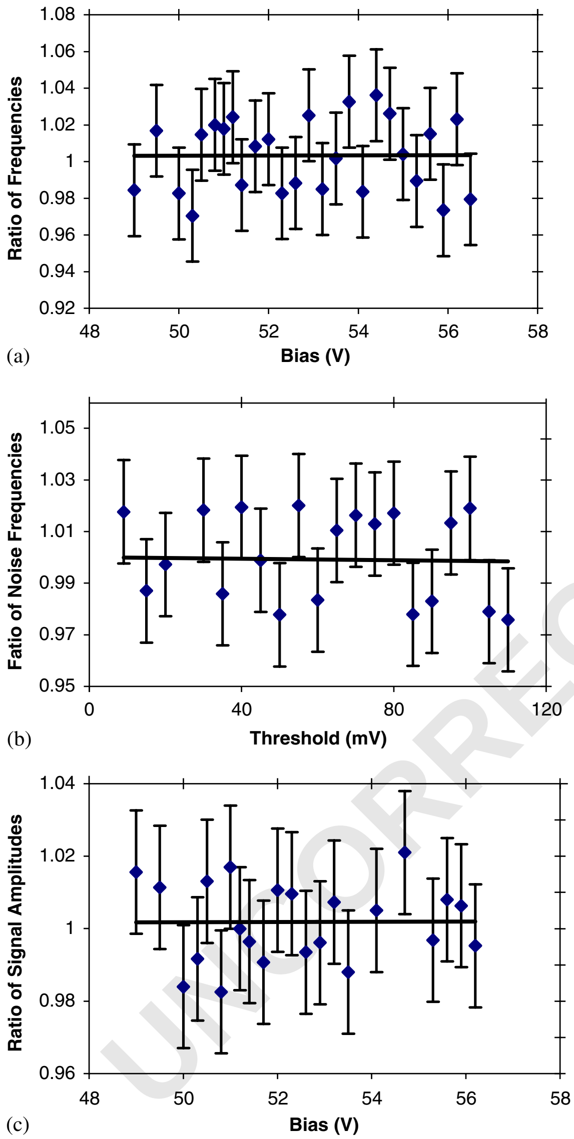


Fig. 7. (a) Ratio of signal + noise count rate as a function of the bias voltage before and after irradiation (threshold set at 80 mV). (b) Ratio of MRS dark noise rate vs. threshold before and after irradiation (MRS biased at 52 V). (c) Ratio of signal amplitude vs. bias voltage before and after irradiation.

### 2.5. LED measurements

The apparatus shown in Fig. 8 was used to perform calibration measurements. In order to closely simulate the output of the scintillating cell, a blue (maximum output at ~450 nm) LED was used. The LED was positioned such that its light was illuminating a KURARAY [6] Y-11, 1 mm, round, ~1 m long wavelength shifting (WLS) fiber perpendicularly to its optical axis, ensuring that blue light did not reach the photodetector directly. A LeCroy [4] 623B octal discriminator, ORTEC [5] delay line and LeCroy [4] 2249A 12-channel ADC were used to process the signal.

The MRS was biased at 52.0 V. Fig. 9 shows the sensor response to the LED signal. We see clear

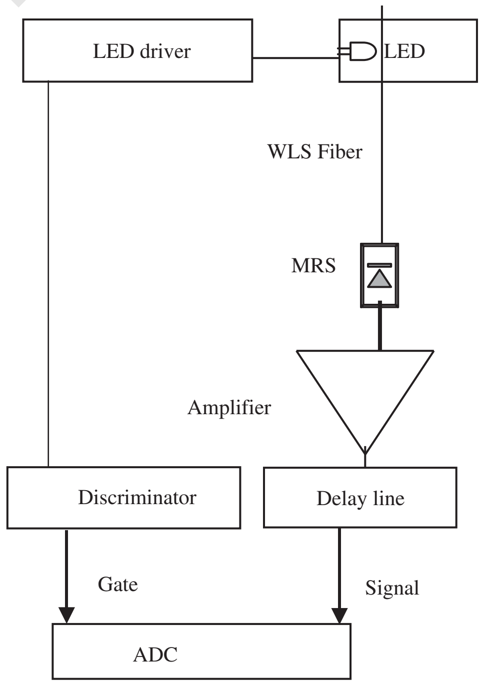


Fig. 8. Setup used for LED measurements.

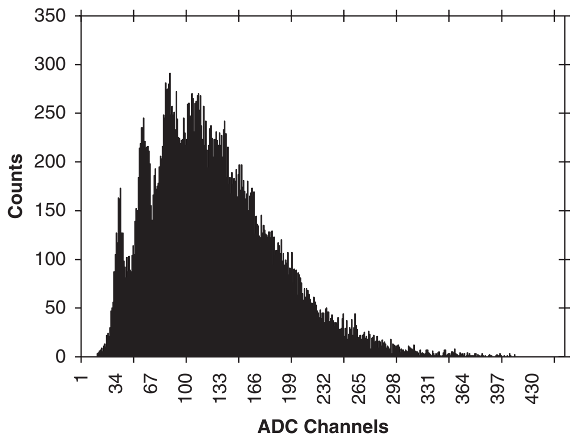


Fig. 9. MRS response to LED signal. MRS was biased at 52.0 V and a gate of ~50 ns used. Pedestal was in channel 38.

single-electron separation, and the first few photo-electrons are easily distinguishable. According to fits, the number of ADC channels between the pedestal and the first PE is the same as between the first and second PE, the second and third PE, and so on.

### 2.6. *Cosmic ray and radioactive source measurements*

A test was also performed using a scintillating strip with cosmic rays as the source of minimum ionizing particles (MIPs). The strip used was made from an extruded scintillator with a co-extruded hole [7] along the strip that was 1 m long, 5 cm wide and 5 mm thick. A 1.15 m long KURARAY [6] Y-11, 1.0 mm outer diameter, round, multiclad, WLS fiber with mirrored end, was embedded and glued, with 0.15 m of fiber from the end of the strip to the MRS. The MRS was biased at 52.0 V, and a gate of ~50 ns and a double-coincidence trigger were used. Fig. 10 illustrates the apparatus used for the cosmic ray measurements. Fig. 11a shows the cosmic ray signal collected with the MRS. Using calibration data from the LED measurements for the position of first PE, we estimate the signal level at 17 PE.

In addition, measurements were conducted using a $^{106}$Ru radioactive source. For this measurement, a hexagonal 9 cm$^2$ and 5 mm thick cell from an extruded scintillator with a sigma shaped fiber groove was used. A 1 m long, KURARAY [6] Y-11, 1.0 mm outer diameter, round, multiclad, WLS fiber with mirrored end, was embedded and glued. Fig. 11b shows the cosmic ray signal collected with the MRS. Using calibration data from above, we estimate the signal level at ~23 PE.

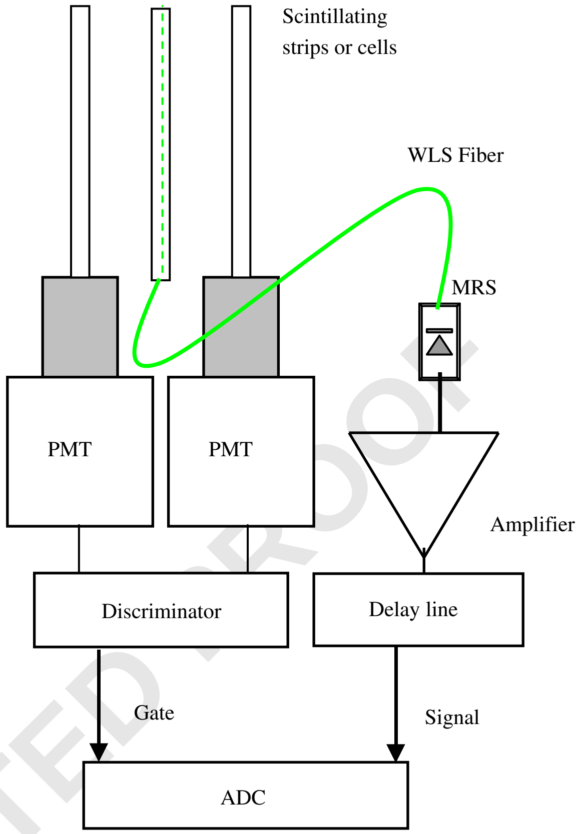


Fig. 10. Setup used for cosmic ray measurements.

### 2.7. *Fiber positioning and sensor response*

The dependence of the MRS output on the fiber-sensor alignment was studied. Scans were conducted with the fiber being moved along, away and positioned at an angle to the sensor. A block diagram of the experimental setup is shown in Fig. 1. Light signals from the green LED (peak emission at ~510 nm) via a 40 cm long clear fiber

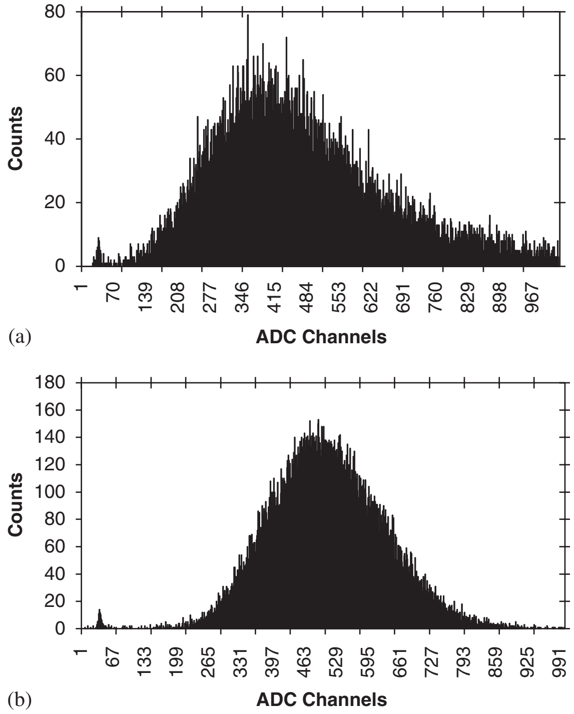


Fig. 11. (a) MRS response to scintillating strip signal from cosmic rays. MRS was biased at 52.0 V and a gate of ~50 ns used. Pedestal was in channel 38. The average yield is 17 PE. (b). MRS response to scintillating cell signal from $^{106}Ru$. MRS was biased at 52.0 V and a gate of ~50 ns used. Pedestal was in channel 38. The average yield is 23 PE.

were supplied to the MRS and the response was measured using a Tektronix [8] TDS2024 oscilloscope. The position and movements of the fiber with respect to the sensor were achieved and measured with a Newport [9] 462 series XYZ-M integrated linear stage (Fig. 12). This stage allows linearity of travel accuracy of 100 μrad about any axis and reproducible return to the same point within an accuracy of $\pm 2.5\,\mu m$. For all of the following tests, unless stated otherwise, a 0.5 mm outer diameter clear fiber was used and the sensor itself was biased at 52 V.

Fig. 13 shows the normalized MRS response as a function of the fiber position relative to the sensor. The plateau corresponds to the region where the entire area of the fiber is within the photosensitive area of the sensor. Long tails on the far right and left sides are due to light reflection off the protective shielding and the mount of the sensor; thus a very small, but non-zero, value of the response is observed when the fiber moves completely away from the photosensitive area of the MRS. Also the fiber is not pressed firmly onto the sensor area. Hence, as the light signal exits the fiber, it forms a cone with somewhat larger cross-

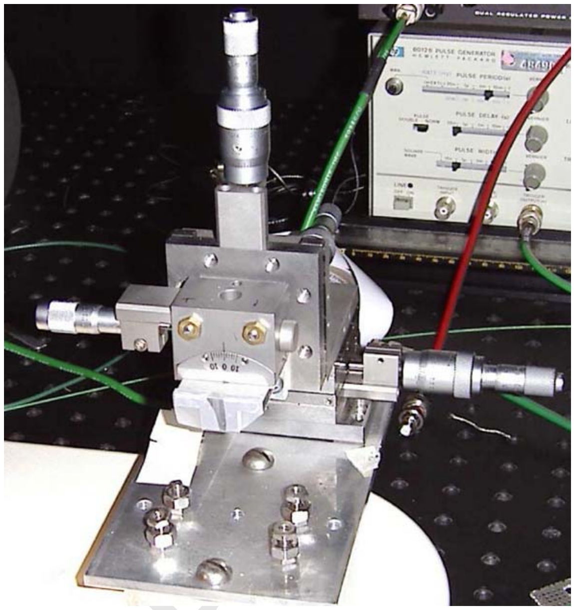

Fig. 12. 462 series XYZ-M device.

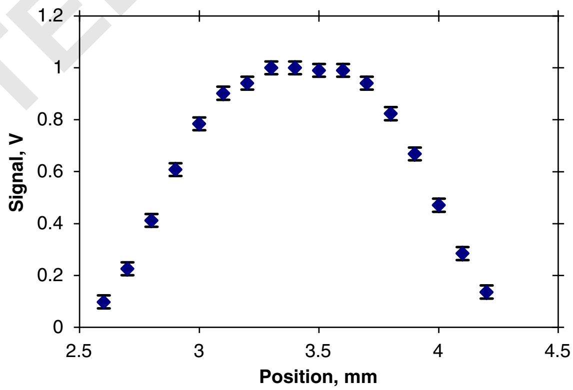


Fig. 13. Output signal amplitude vs. position of the fiber along the MRS sensor. Output is normalized to the peak value.

section at the surface of the sensor than the fiber itself would present. Precision of these measurements is approximately $\pm 12\,\text{mV}$ at each point. Positioning accuracy is $\pm 2.5\,\mu\text{m}$. These uncertainties are the same for all plots.

In addition, measurements of the output signal amplitude versus the distance of the fiber away from the sensor were performed. Fig. 14 shows the results for this scan. The point at 0 mm corresponds to the fiber in physical contact with the MRS surface. The scan was performed with the fiber positioned in the approximate center of the photosensitive area of the sensor, well within the plateau region (Fig. 13).

The dependence of the output signal on the fiber angle to the sensor was also measured. Fig. 15 shows the result of that scan. Finally, a scan was performed along the sensor with the fiber tilted at $\alpha = 1^\circ$. Results of that scan are shown in Fig. 16. The direction of the scan is the same as in Fig. 13. As expected, the curve shows a slight asymmetry.

### 2.8. Linearity of response

We have also explored the linearity of the MRS response as the intensity of the incident light increases. The apparatus from Fig. 1 was used in this test with the oscilloscope connected to the output of the amplifier without a discriminator and counter. Generator pulses of $\sim$10 ns were used. Since the MRS is a multi-pixel device, it is

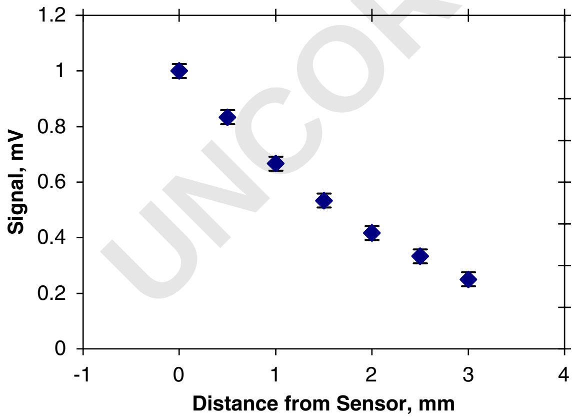


Fig. 14. Output signal amplitude vs. fiber distance from the sensor. Output is normalized to the peak value.

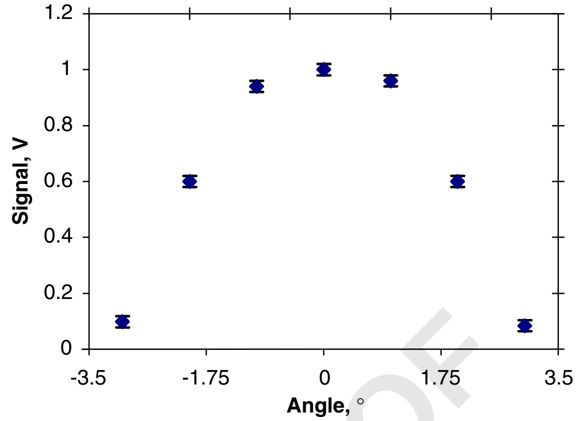


Fig. 15. Output signal amplitude vs. angle of the 0.5 mm fiber to the MRS sensor surface. Output is normalized to the peak value.

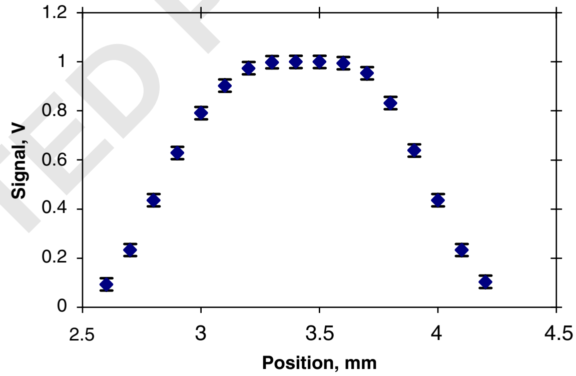


Fig. 16. Output signal amplitude vs. position of the tilted 0.5 mm fiber. Output is normalized to the peak value.

natural to expect that the deviation from the linearity of response will be observed when a substantial amount of the pixels have fired simultaneously. As a reference device to measure the incident light intensity, a Hamamatsu [10] S8550 avalanche photodiode (APD) was used. The results of this measurement are presented in Fig. 17. The vertical axis is the ratio of observed MRS response to different levels of incident light, to the values that would have been if the response were strictly linear. These values are estimated by extrapolating a straight line fit to the first few

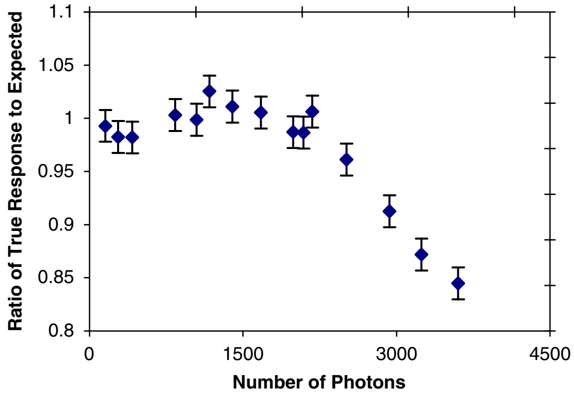


Fig. 17. MRS response vs. the intensity of incident light signal. The *x*-axis indicated a number of incident photons, with the MRS detection efficiency being ~25%.

points. The horizontal axis is calibrated in the number of incident photons as detected by the APD.

From Fig. 17, a deviation from linearity at the level of 5% starts at ~2200 incident photons (~550 PE in MRS response), and a deviation of <10% with light intensity up to ~3000 photons (~750 PE). From Fig. 11, one MIP signal on average corresponds to 17 PE; thus, within 5% of linearity, up to 32 MIPs can be detected.

## 3. Conclusions

MRS photodiodes represent a new generation of photosensors. We have conducted a set of measurements to illustrate the potential use of these sensors in high-energy physics detectors. As can be seen, the MRS is a promising photodetector for scintillator-based multi-channel readout systems.

Each sensor requires determination of a working point (an optimal bias voltage) to ensure balance between amplification and detection efficiency with the noise level. Within one production batch, the dispersion of working point value is small (<1%).

At each given bias voltage the noise level can be greatly reduced by imposing a threshold. For instance, at the working point, the threshold at 1 PE level reduces noise by a factor of 2500. Our study indicates that MRS noise is dominated by single PE noise.

The irradiation study shows that 1 Mrad dose of gamma radiation has no noticeable effects on the MRS performance. Temperature measurements indicate an inverse dependence of the output signal amplitude on temperature. The drop in noise frequency is exponential with decreasing temperature.

Tests of fiber misalignment with the sensor were carried out as well. The fiber tilt of 1° with respect to the normal to the sensor's surface reduced the MRS output by ~4%, whereas an air gap of 0.5 mm between the sensor and the fiber accounts for ~16% of signal loss. In addition, if the area of the fiber is comparable with the photosensitive area of the sensor, the alignment of the fiber becomes an important issue.

The response of the sensor is linear over a reasonable range of light input, with a 5% deviation starting at ~2200 incident photons. Using strips made from an extruded scintillator, we see 17 PE per MIP. Thus, up to 32 MIPs can be detected when the sensor is operating in the linear regime. The substantial photoelectron/MIP yield of the MRS when used with either a long strip or a small tile illustrates their great potential in particle detectors.

## Acknowledgment

We thank Victor Golovin for useful discussions. Also we express our gratitude to Robert D. Angstadt for software troubleshooting.

## References

[1] A. Dyshkant, D. Beznosko, G. Blazey, D. Chakraborty, K. Frances, D. Kubik, et al., "Small Scintillating Cells as the Active Elements in a Digital Hadron Calorimeter for the e+e− Linear Collider Detector", FERMILAB-PUB-04/015,9 February , 2004.
[2] V. Golovin, et al., Nucl. Phys. Proc. Suppl. B 61 (1998) 347.
[3] M. Golovin, et al., Nucl. Instrum. and Meth. A 387 (1997) 231.

[4] LeCroy Corporation, 700 Chestnut Ridge Road, Chestnut Ridge, NY, 10977-6499
[5] ORTEC, 801 South Illinois Avenue, Oak Ridge, TN 37830
[6] Kuraray America Inc., 200 Park Ave, NY 10166,USA; 3-1-6, Nihonbashi, Chuo-Ku, Tokyo 103-8254, Japan.
[7] Anna Pla-Dalmau, Alan D. Bross, Victor V. Rykalin, "Extruding Plastic Scintillator at Fermilab", FERMILAB-Conf-03-318-E, October 2003.
[8] Tektronix Inc, 14200 SW Karl Braun Drive, P.O. Box 500, Beaverton, OR, 97077 USA.
[9] Newport Corporation, 1791 Deere Avenue, Irvine, CA, 92606 USA.
[10] Hamamatsu Corporation, 360 Foothill Road, P.O. Box 6910, Bridgewater, NJ 08807-0919, USA; Shimokanzo 314-5, Toyooka-village, Iwata-gun, Shizuoka-ken, 438-0193 Japan.